A Second Earth-sized Planet in the Habitable Zone of the M Dwarf, TOI-700

Emily A. Gilbert[1] , Andrew Vanderburg[2] , Joseph E. Rodriguez[3] , Benjamin J. Hord[4,5] , Matthew S. Clement[6,7] ,
Thomas Barclay[5,8] , Elisa V. Quintana[5] , Joshua E. Schlieder[5] , Stephen R. Kane[9] , Jon M. Jenkins[10] ,
Joseph D. Twicken[10,11] , Michelle Kunimoto[2] , Roland Vanderspek[2] , Giada N. Arney[5,12] , David Charbonneau[13] ,
Maximilian N. Günther[14,24] , Chelsea X. Huang[15] , Giovanni Isopi[16] , Veselin B. Kostov[5,11] , Martti H. Kristiansen[17] ,
David W. Latham[18] , Franco Mallia[16] , Eric E. Mamajek[1] , Ismael Mireles[19] , Samuel N. Quinn[18] , George R. Ricker[2] ,
Jack Schulte[3] , S. Seager[2,20,21] , Gabrielle Suissa[22] , Joshua N. Winn[23] , Allison Youngblood[5] , and Aldo Zapparata[16]

[1] Jet Propulsion Laboratory, California Institute of Technology, 4800 Oak Grove Drive, Pasadena, CA 91109, USA; emily.a.gilbert@jpl.nasa.gov
[2] Department of Physics and Kavli Institute for Astrophysics and Space Research, Massachusetts Institute of Technology, Cambridge, MA 02139, USA
[3] Center for Data Intensive and Time Domain Astronomy, Department of Physics and Astronomy, Michigan State University, East Lansing, MI 48824, USA
[4] University of Maryland, College Park, MD 20742, USA
[5] NASA Goddard Space Flight Center, 8800 Greenbelt Road, Greenbelt, MD 20771, USA
[6] Earth and Planets Laboratory, Carnegie Institution for Science, 5241 Broad Branch Road, NW, Washington, DC 20015, USA
[7] Johns Hopkins APL, 11100 Johns Hopkins Rd, Laurel, MD 20723, USA
[8] University of Maryland, Baltimore County, 1000 Hilltop Circle, Baltimore, MD 21250, USA
[9] Department of Earth and Planetary Sciences, University of California, Riverside, CA 92521, USA
[10] NASA Ames Research Center, Moffett Field, CA 94035, USA
[11] SETI Institute, Mountain View, CA 94043, USA
[12] GSFC Sellers Exoplanet Environments Collaboration, NASA Goddard Space Flight Center, Greenbelt, MD 20771, USA
[13] Center for Astrophysics | Harvard & Smithsonian, 60 Garden Street, Cambridge, MA 02138, USA
[14] European Space Agency (ESA), European Space Research and Technology Centre (ESTEC), Keplerlaan 1, 2201 AZ Noordwijk, The Netherlands
[15] University of Southern Queensland, West St, Darling Heights, Toowoomba, Queensland, 4350, Australia
[16] Campo Catino Astronomical Observatory, Regione Lazio, Guarcino (FR), I-03010 Italy
[17] Brorfelde Observatory, Observator Gyldenkernes Vej 7, DK-4340 Tølløse, Denmark
[18] Center for Astrophysics | Harvard & Smithsonian, 60 Garden St, Cambridge, MA, 02138, USA
[19] Department of Physics and Astronomy, University of New Mexico, 210 Yale Blvd NE, Albuquerque, NM 87106, USA
[20] Department of Earth, Atmospheric and Planetary Sciences, Massachusetts Institute of Technology, Cambridge, MA 02139, USA
[21] Department of Aeronautics and Astronautics, MIT, 77 Massachusetts Avenue, Cambridge, MA 02139, USA
[22] Department of Astronomy and Astrobiology Program, University of Washington, Box 351580, Seattle, Washington 98195, USA
[23] Department of Astrophysical Sciences, Princeton University, Princeton, NJ 08544, USA

Abstract

We report the discovery of TOI-700 e, a 0.95 $R_\oplus$ planet residing in the Optimistic Habitable Zone (HZ) of its host star. This discovery was enabled by multiple years of monitoring from NASA's Transiting Exoplanet Survey Satellite (TESS) mission. The host star, TOI-700 (TIC 150428135), is a nearby (31.1 pc), inactive, M2.5 dwarf ($V_{\mathrm{mag}} = 13.15$). TOI-700 is already known to host three planets, including the small, HZ planet, TOI-700 d. The new planet has an orbital period of 27.8 days, and based on its radius (0.95 $R_\oplus$), it is likely rocky. TOI-700 was observed for 21 sectors over Years 1 and 3 of the TESS mission, including 10 sectors at 20 s cadence in Year 3. Using this full set of TESS data and additional follow-up observations, we identify, validate, and characterize TOI-700 e. This discovery adds another world to the short list of small, HZ planets transiting nearby and bright host stars. Such systems, where the stars are bright enough that follow-up observations are possible to constrain planet masses and atmospheres using current and future facilities, are incredibly valuable. The presence of multiple small, HZ planets makes this system even more enticing for follow-up observations.

1. Introduction

The field of exoplanets has come great lengths over the past several decades. In the early days of exoplanet science, the focus was largely on individual planet detections, showing that these worlds even exist and that astronomers are capable of detecting them. The first planets detected were truly alien: planets orbiting pulsars, blisteringly hot worlds orbiting their

host stars in just a few days, or giant planets more massive than any seen in our Solar System (e.g., Wolszczan & Frail 1992; Mayor & Queloz 1995; Bouchy et al. 2005). The nascent technology used in the early days of exoplanet discovery, however, prevented the detection of smaller planets, orbiting farther from their main-sequence host stars.

In the 2000s and 2010s, the introduction of new technology and facilities pushed the field closer to discovering Solar System analogs. The High Accuracy Radial-velocity Planet Searcher (HARPS; Mayor et al. 2003) used the Doppler method to reveal a huge population of sub-Neptune-mass exoplanets orbiting close to their stars (Mayor et al. 2011). The launch of space missions like MOST (Walker et al. 2003), CoRoT (Auvergne et al. 2009), and Kepler (Borucki et al. 2010)

---

delivered the sensitivity to detect even smaller planets using the transit method. The Kepler mission in particular observed with high enough sensitivity to routinely detect Earth-sized planets on temperate orbits around M-dwarf stars, leading to the discovery of the first Earth-sized HZ planet (Kepler 186-f; Quintana et al. 2014). Analysis of the ensemble of Kepler's planetary discoveries led to the realization that multi-planet systems are common, often have flat, coplanar architectures like that of our Solar System, and perhaps most profoundly, that HZ Earth-sized planets are common (Dressing & Charbonneau 2013; Petigura et al. 2013; Dressing & Charbonneau 2015; Bryson et al. 2021). Despite these break-throughs, Kepler targets were limited by the fact that most of Kepler's planetary discoveries orbited stars too faint for detailed characterization using other telescopes on the ground or in space. Without knowledge of their bulk compositions and atmospheres, it was impossible to discern whether the habitable-zone Earth-sized planets Kepler found in spades were truly Earth-like.

Fortunately, Kepler's direct successor, the Transiting Exoplanet Survey Satellite (TESS) mission (Ricker et al. 2015), offers an opportunity to fill in the gaps in knowledge left by Kepler. TESS operates using a different observing strategy from Kepler—tiling the entire sky in 28 days long observations called sectors. TESS observes an area of sky that is 400 times greater than that surveyed in Kepler's primary mission, and it is specifically targeting Earth's nearest stellar neighbors. One challenge resulting from TESS's observing strategy is that the shorter observation periods make it difficult to discover multi-planet systems with long-period planets. Fortunately, near the ecliptic poles, the TESS fields of view for each sector overlap, forming Continuous Viewing Zones (CVZs), enabling longer stares at targets. These longer stares allowed for the discovery and characterization of prominent TESS multi-planet systems such as L 98-59 (Kostov et al. 2019a) and TOI-270 (Van Eylen et al. 2021).

One notable discovery from TESS is the TOI-700 system of planets. TOI-700 is an M2.5 dwarf[25] that resides in TESS's Southern CVZ. In 2020, this system was shown to host three planets, including the first HZ, Earth-sized planet found using TESS data, TOI-700 d (Gilbert et al. 2020; Rodriguez et al. 2020). Given the relative scarcity of small, temperate worlds currently known, TOI-700 d makes this system a particularly intriguing target of its own merit. Here, we introduce a fourth planet, TOI-700 e, orbiting between planets TOI-700 c and TOI-700 d, residing within the Optimistic HZ (Kopparapu et al. 2013). There are only around a dozen small, HZ planets known to date, so this second HZ planet within a single system further emphasizes the importance of the TOI-700 system for future study.

In this paper, we first describe the observations taken by TESS in Years 1 and 3 of the mission, as well as a ground-based observation of the new planet candidate (Section 2). Next, we vet the planet using difference imaging and statistically validate the planet using vespa in Section 3. After showing that TOI-700 e is almost certainly a bona fide planet, we then fit all four planets in the system in Section 4, providing updated planet parameters from Gilbert et al. (2020) and Rodriguez et al. (2020) for planets b, c, and d. In Section 5,

we discuss the expected properties of planet e as well as prospects for follow-up. We also study the dynamical properties of the system and compare this system to other known multi-planet systems. Finally, we summarize the paper in Section 6.

2. Observations

We obtained data from the ongoing TESS mission, which observed TOI-700 in Years 1 and 3 of operation. These observations are described in detail in Section 2.1. We also conducted ground-based observations to rule out astrophysical false-positive scenarios for planet e with Campocatino Austral Observatory, which are described in Section 2.2. We also took advantage of the wealth of data collected by Gilbert et al. (2020) and Rodriguez et al. (2020), who characterized the host star and validated planets b, c, and d.

2.1. TESS Observations

TOI-700 resides in the TESS Southern CVZ and was observed for extended stretches of TESS Years 1 and 3 of observations. During Year 1, TOI-700 was observed at 2 minutes cadence during Sectors 1, 3, 4, 5, 6, 7, 8, 9, 10, 11, and 13, as a result of its inclusion in Guest Investigator Program Cycle 1 proposal G011180 (PI: C. Dressing).[26] TOI-700 was observed at short cadence in Year 3 of observations, as a result of its inclusion in a number of Guest Investigator (GI) Programs: G03183 (PI: J. Rodriguez); G03264 (PI: J. Van Saders); G03278 (PI: A. Mayo); and G03068 (PI: D. Kipping). In particular, we present this work as a part of the approved GI program G03183 (PI: J. Rodriguez), which enabled TOI-700 to be observed at 20 s cadence in Year 3 of observations. In Year 3, TOI-700 was observed during Sectors 27, 28, 30, 31, and 33–38. Sectors missing in both years of TESS observations are a result of the target falling within the gaps of the detectors.

A search of the TESS Year 1 data revealed three transiting planet candidates. Gilbert et al. (2020) used these data coupled with follow-up observations to validate the three candidates as bona fide planets called TOI-700 b, c, and d. After the Year 3 data were collected, a search of the full data set revealed an additional transiting planetary candidate orbiting interior to TOI-700 d, which we refer to in this paper as TOI-700 e. TOI-700 e transited seven times during the first year of observations and another seven times during the third year of observations (six of which were uncontaminated by transits of other planets). The transits of TOI-700 e are somewhat shallower than those of TOI-700 d, which explains why it was not detected in the first year of observations alone, despite orbiting interior to the previously known TOI-700 d.

The signal of TOI-700 e was first detected as a threshold crossing event (TCE), as a part of the TESS Science Processing Operations Center (SPOC; Jenkins et al. 2016) Sectors 1–39, multi-sector transit search conducted on 2021 July 31. The SPOC pipeline searches for planets using the Transiting Planet Search (TPS) software, which is an adaptive, noise-compensating matched filter (Jenkins et al. 2002, 2010, 2020). After detection by TPS, TOI-700 e passed all the diagnostic tests exercised and was reported in the Data Validation reports (Twicken et al. 2018; Li et al. 2019), including the difference image centroiding test, which located the source of this transit

signature to within $6\rlap{.}''4 \pm 3\rlap{.}''6$ of TOI-700. After reviewing the DV reports and other diagnostics, the TESS Science Office issued an alert upgrading this from a TCE to a TOI (TOI-700.04) on 2021 November 19 (Guerrero et al. 2021).

In order to maximize the signal-to-noise ratio of the shallow transits of TOI-700 e, we generated custom light curves from the target pixel files (TPFs) for the target and used those light curves for our transit fits. We used 20 s cadence data when it was available (Year 3 data), which yielded higher precision than the 2 minutes cadence data for the same time period. We re-extracted the light curves from the TPFs using the systematics corrections described in Vanderburg et al. (2019). In addition to decorrelating against the quaternion time series, we also decorrelated against the Co-trending Basis Vectors (CBVs) that are generated by the SPOC pipeline's Presearch Data Conditioning (PDC, Smith et al. 2012; Stumpe et al. 2012, 2014) module. We elected not to decorrelate against the time series with the high-pass-filtered background levels as is sometimes done; including the background time series into our regression introduced artifacts into the final light curves. Finally, for each sector, we sampled 20 different apertures and chose the one that minimized photometric scatter to use for extracting the photometry. We use this light curve for our analysis going forward.

2.2. Campocatino Austral Observatory

On 2021 December 27 UT, we observed an egress of the transit of TOI-700 e using the CAO (Campocatino Austral Observatory), situated at El Sauce Observatory in Chile and supported by the Obstech remote telescope hosting facility.[27] The CAO is a 61 cm diameter, Planewave CDK24" telescope, and the observation was conducted by taking 360 s exposures using a clear filter. The goal was to identify or rule out the existence of any nearby eclipsing binary stars blended with TOI-700 in TESS's images that could have contributed the signal of TOI-700 e. Following the guidelines from the TESS Follow-up Observing Program Working Group (TFOP WG) Sub Group 1 (SG1), which conducts follow-up photometric observations of TESS planet candidates, we considered a target to be "cleared" (shown definitively not to be an eclipsing binary contaminant) if the NEBdepth (the depth of an eclipse needed to cause the transit signal) is greater than or equal to five times the root mean square scatter in the star's light curve (NEBdepth/rms $> = 5$). Likewise, if the NEBdepth is between three and five times the root mean square scatter, we consider the star "likely cleared." With these data, we cleared or likely cleared 66 out of 86 stars within $2\rlap{.}'5$ with no obvious nearby eclipsing binaries detected.

3. Vetting

We have conducted several statistical analyses in order to ensure that the signals are real, following the methods Gilbert et al. (2020) used to validate TOI-700 b, c, and d. False-positive planet candidates can come in several flavors, including astrophysical signals (eclipsing binaries) hosted by nearby known blended stars, astrophysical signals from very close and unknown blended stars, and instrumental artifacts. Validating planets is defined as retiring almost all of these potential false-positive scenarios so that the probability that the

transit signal is a false positive is very low (typically below 10^{-2}). In this section, we perform tests to assess the likelihood that the signal from the new candidate is due to any of these sources. In particular, we performed extensive consistency tests to determine that the signal is not driven by a handful of ill-timed instrumental artifacts (Section 3.1). We also used difference imaging (Section 3.2) to study the signal from the star at the pixel level in order to rule out eclipsing binaries from stars more than a few arcseconds away and discern whether or not the transits occur on target. Finally, we employed vespa (Section 3.3) to determine the astrophysical false-positive probability for the planet and assess the likelihood that the signal is caused by very closely blended companions.

3.1. Vetting for Instrumental Artifacts

Small planets are notoriously difficult to detect, due to their shallow transits and correspondingly low S/N. This was especially true during the Kepler mission, but is also a known problem for the TESS mission where numerous low-Multiple Event Statistic (MES, a proxy for S/N reported by TPS) TOIs have later been found to be false alarms due to instrumental systematics. In such instances, it is generally best practice to confirm planet candidates using an independent facility, as was done for TOI-700 d with Spitzer (Rodriguez et al. 2020). Unfortunately, Spitzer was decommissioned in early 2020, and it is no longer available for planet follow-up. Moreover, the CHEOPS (Benz et al. 2021) spacecraft, which has shouldered some of the observational burden left by Spitzer's decommissioning, cannot observe TOI-700 because the star is too far south from the ecliptic plane.

In the absence of available spacecraft for follow-up, we are forced to instead rely solely on the TESS data in order to validate TOI-700 e. The MES of this detection is 7.2, which is barely above the customary detection threshold of 7.1 (Guerrero et al. 2021). We therefore performed an analysis to obtain a more accurate signal-to-noise ratio than the estimate from the MES, using an optimized transit shape and including every transit in the analysis. Our S/N calculation also incorporated red noise in order to assess how vulnerable we are to instrumental effects. We did this using a matched filter approach; we took the best-fit transit model from our exofast global analysis described in Section 4 and convolved it with the light curve of TOI-700. We subtracted the best-fit models for planets b, c, and d prior to performing the convolution, and we were able to recover two additional transits that previously overlapped with transits of other planets in the system. This analysis resulted in a signal from TOI-700 e that produced a strong peak in the matched filter response when folded on the expected period and transit epoch of the signal. Compared to the scatter of the matched filter response out-of-transits, we find that TOI-700 e's signal has a significance of 10.05σ. While signals with significance greater than 10σ are generally unlikely to be instrumental artifacts, TOI-700 e just barely surpasses that threshold. It should be noted that this analysis is equivalent to the "mod-shift" test used by the Kepler Robovetter software and in the DAVE package.

We also performed this same analysis on subsets of the data, to test the growth of the signal as new transits were observed by TESS. We started by only analyzing data up to the first transit, then iteratively added each subsequent transit of planet e. We then plotted the significance of the peak in the matched filter response as a function of observed transit number. We found

---

[27] https://obstech.cl/
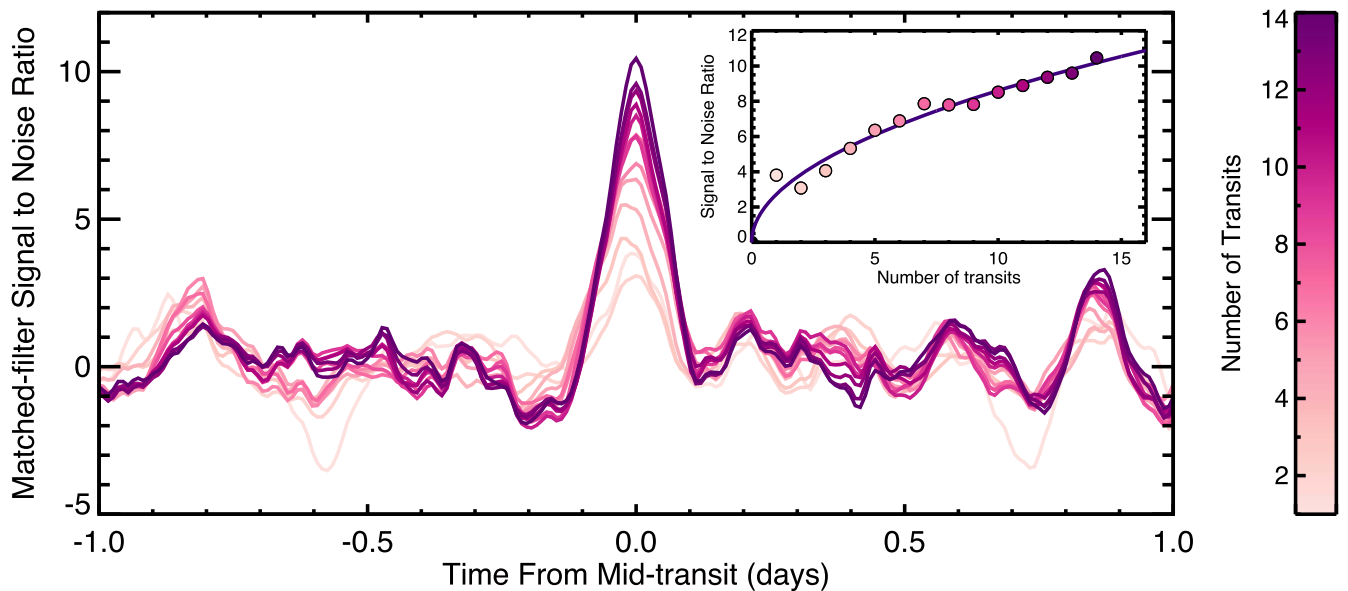
Figure 1. Signal-to-noise ratio of TOI-700 e's transit detection as a function of number of observed transits. The main panel shows matched-filter response functions of a filter shaped like TOI-700 e's transit convolved with the TOI-700 light curve. The individual curves show the response of the light curve as additional data were collected. Curves with only a small number of transits (light pink) show a relatively weak detection of the planet's signal, while curves with many observed transits show a convincing detection, with greater than 10σ significance. The inset shows the peak signal-to-noise ratio of the planet's signal as a function of the number of observed transits. The purple curve is a best-fit curve with a square root power law, which describes the growth of the signal strength well, as expected for an astrophysical transit signal. The consistent growth of the signal-to-noise ratio as additional data was collected is evidence that the signal of TOI-700 e is not dominated by occasional instrumental artifacts, and instead is caused by a periodic signal with a period of 27.8 days. We note that, in the parlance of Kepler exoplanet detection literature, this type of metric is known as a "mod-shift" test.
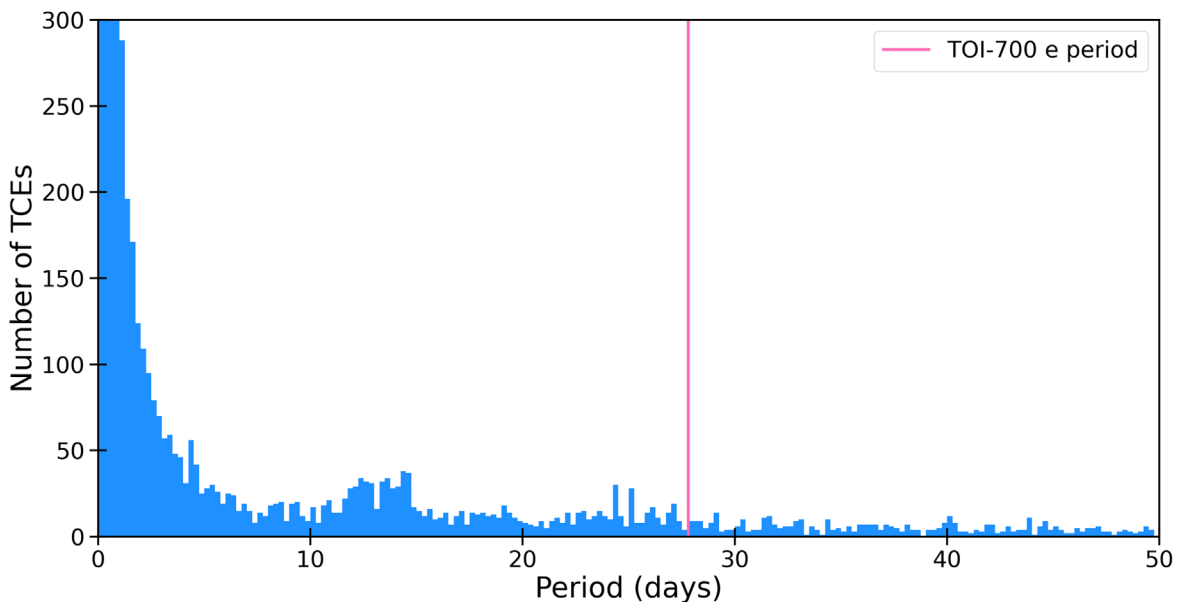
Figure 2. The distribution of periods of the TCEs shows that there is no significant pileup at the period of TOI-700 e (27.8 days) in this cutaway figure. The lack of overdensity at this period implies that there is no instrumental effect inducing planet signals at the period of TOI-700 e.

that the significance grows over time, and it increases with each additional observed transit (see Figure 1). This growth is consistent with a square-root curve, as would be theoretically expected for a real, periodic signal such as a planet transit. If the signal were caused by instrumental artifacts, they must be periodic with a 27.8 day period and each event must be relatively consistent in amplitude; if the signal were not repeating periodically with consistent amplitude, we would not see the growth in significance in this manner. We also checked

the distribution of all TCEs detected by TESS, to see if similar signals are present in other stars, which would imply an instrumental origin for both those signals and TOI-700 e. There is no significant overdensity of detected TOI or TCE signals with a period identical to 27.8 days; see Figure 2. These results, coupled with the 14 transits of TOI-700 e observed by TESS spread over three years, strongly disfavor a signal of instrumental origin, thus implying that TOI-700 e's signal is indeed astrophysical.

3.2. Difference Imaging

A common type of false positive is a nearby eclipsing binary (NEB) that contaminates the aperture pixels, causing the target light curve to show a transit-like signal. We used difference imaging in order to assess the evidence for this sort of contamination in the TESS pixel-level data.

We first employed DAVE (Discovery and Vetting of Exoplanets; Kostov et al. 2019b) to study the potential sources of contamination. However, the combination of low S/N and long period of of the planet makes robust vetting with the DAVE pipeline unreliable for this target. Given there is at most one transit per sector, both the photocenter and the light-curve modules of DAVE are vulnerable to cross-sector systematic effects. For example, non-astrophysical depth differences between different sectors would mislead the modshift module in interpreting two consecutive transits as exhibiting odd–even differences and flagging the planet candidate as a false positive. Without a definitive assessment from DAVE, we went on to use additional difference imaging to further vet this new planet candidate.

We then used the SPOC difference image centroid offsets (Twicken et al. 2018), which are averaged over all sectors in the Sectors 1–39 transit search, in order to confirm that the transit occurred on target (within $6\rlap{.}''4 \pm 3\rlap{.}''6$ of TOI-700). No other stars bright enough to cause the transit signal of TOI-700 e lie within this region of sky, so this result implies that TOI-700 e's signal must be coming from either TOI-700 itself, or an unknown star blended with TOI-700. We verified this result using the difference imaging technique from Bryson et al. (2013) as implemented in the Python package tess-plots.[28] This method also confirmed that the transit occurred on target. The TESS Data Validation Reports also provide odd/even transits, and we inspected these and confirm that the depths match (consistent at the 0.83 sigma level), indicating that we are not seeing secondary eclipses of the planet candidate.

3.3. Statistical Vetting with vespa

Although follow-up observations can rule out portions of parameter space where astrophysical false positives may exist, these observations are incomplete and do not yet definitively rule out the possibility that TOI-700 e's signal is an astrophysical false positive. Therefore, we supplemented our follow-up observations with a statistical analysis of the remaining likelihood of astrophysical false-positive scenarios using the publicly available software package vespa (Morton 2012, 2015), in order to establish the planetary nature of this signal.

vespa compares the transit signal to a number of astrophysical false-positives including an unblended eclipsing binary (EB), a blended background EB (BEB), a hierarchical companion EB, and EB scenarios with a double period. The software assumes priors on the binary star occurrence rate from Raghavan et al. (2010), direction-specific star counts from Girardi et al. (2005), and planet occurrence rates from Morton (2012) before forward-modeling simulated populations for each category of false-positive scenario. The known eclipse depth, duration, and ingress duration for these simulated populations are then compared against photometric data and

planetary and orbital parameters provided by the user to calculate the likelihood that the target signal is well-described by one of these false-positive populations.

We ran vespa using the SPOC-produced light curves, which we phase-folded using the median values of the posteriors for the period and mid-transit time. The transits of the other planets in the TOI-700 system were subtracted from the light curve for this analysis. We included the maximum possible secondary depth of phase-folded features calculated by DAVE (Section 3.2) and the SOAR I-band contrast curve (Gilbert et al. 2020) as observational constraints when calculating the false-positive probability of the TOI-700 e signal. By default, vespa simulates the background starfield within 1 square degree of the target, but we dictated that the maximum aperture radius interior to which the signal must be produced be $42''$, which is the radius of two TESS pixels, and the maximum size of the aperture that the SPOC pipeline used to extract the light curves. vespa assumes that the transit-like signal is on target, which has been confirmed in this case by follow-up observations outlined in Section 2 and the centroid analysis performed in Section 3.2.

Using these inputs, we calculate the false-positive probability (FPP) of the TOI-700 e signal to be 2.74×10^{-4}. All false-positive scenarios have probabilities $\lesssim 10^{-4}$, strongly disfavoring them over the planet scenario. Because the overall FPP $\ll 0.01$, this signal can be considered to be statistically validated by vespa. Furthermore, this FPP does not account for the fact that the TOI-700 e signal is a part of a multi-planet system. Lissauer et al. (2012, 2014) demonstrated that false positives are less likely in multi-planet systems and that the FPPs calculated without accounting for this fact should be treated as upper limits. An analysis of TESS multi-planet systems indicates that this "multiplicity boost" may reduce these FPPs by a factor of ~50× (Guerrero et al. 2021), further reducing the FPP of this planet. Given these results showing that astrophysical false positives are highly unlikely, in addition to our analysis showing that the signal is not consistent with having an instrumental origin, we therefore state that TOI-700 e is almost certainly a bona fide planet.

4. Transit Fits with EXOFASTv2

To refine our understanding of the three known planets in the TOI-700 system and characterize the newly validated TOI-700 e, we globally fit the available photometric observations using the ExofastV2 software package (Eastman et al. 2019). Our strategy generally followed that presented in Section 3 of Rodriguez et al. (2020). We adopted the same priors on M_{star} and R_{star}, $0.419 \pm 0.021\ R_{\odot}$ and $0.417 \pm 0.021\ M_{\odot}$, that were determined from the absolute K_s–mag relations from Mann et al. (2015), because stellar isochrones are unreliable for low-mass host stars. Priors on the T_{eff} and [Fe/H] (3460 ± 65 K and -0.07 ± 0.11 dex) were also included from spectroscopic analysis from the Southern Astrophysical Research (SOAR) telescope (see Section 3.1 of Gilbert et al. (2020)). We included the TOI-700 c follow-up transit from the Las Cumbres Observatory and the two Spitzer follow-up transits of TOI-700 d in Channel 2 on the Spitzer InfraRed Array Camera (IRAC; Fazio et al. 2004) observed on 2019 October 22 UT and 2020 January 05 UT (Program 14314, PI: Vanderburg). See Section 2.2 and 2.3 from Rodriguez et al. (2020) for the data reduction and analysis of the LCO and Spitzer observations. We included both the primary mission (Year 1) and

---

[28] https://github.com/mkunimoto/TESS-plots
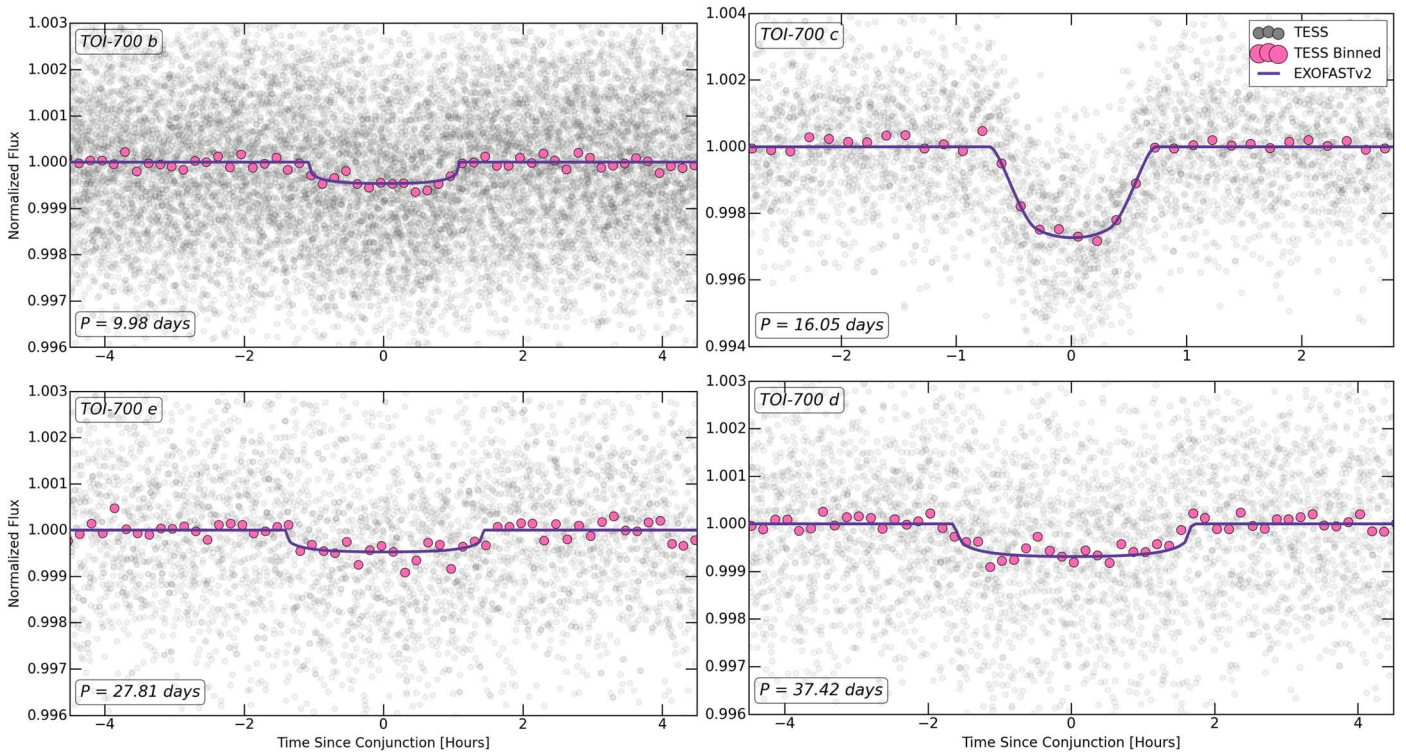
Figure 3. Here, we present the light curves for the TOI-700 planets, phase-folded to each of their orbital periods. The gray dots are the TESS 2 minutes cadence data, the pink dots are the data binned to 10 minutes cadence, and the purple lines show our transit fit generated using EXOFASTv2.

extended mission (Year 3) observations of TOI-700 from TESS. During the extended mission of TESS, TOI-700 was placed on a 20 s cadence target list; these observations yielded higher photometric precision than the 2 minutes cadence data and allowed for a more detailed study of the system. For our global analysis, we binned the 20 s cadence data to 2 minutes and included the primary mission 2 minutes cadence light curve. The results of these fits can be seen in Figure 3 and Table 1 for the stellar parameters, and in Table 2 for the planetary parameters. Table 2 contains both updated parameters for planets b, c, and d, as well as new parameters for planet e. As a result of updated data processing and background subtraction, planets b, c, and d have slightly smaller radii than have been previously reported. We find planet e to be a 0.95 $R_\oplus$ planet on a 27.8 days period orbit. This puts the planet within TOI-700's Optimistic HZ (Kopparapu et al. 2013), receiving 1.27× Earth's insolation flux ($S_\oplus$).

5. Discussion

Here, we describe the potential properties of TOI-700 e and evaluate the system as a whole. We discuss prospects for planet habitability and comment on the dynamical properties of the system. We also compare these planets to other known multi-planet systems, to provide additional context for the TOI-700 system.

5.1. Expected Properties of TOI-700 e

We used the Chen & Kipping (2017) mass–radius relation-ship and the `forecaster` Python package to investigate the likely composition of TOI-700 e. With a radius of 0.953 $R_\oplus$, we found that TOI-700 e is likely a rocky planet with a probability of 87%. `forecaster` yields a mass estimate of $0.845^{+0.67}_{-0.34}$ $M_\oplus$. Using this calculated mass, we estimate the expected RV

Table 1
Median Values and 68% Confidence Intervals for the Global Models for the TOI-700 Stellar Parameters

Parameter	Description (Units)	Median	$+1\sigma$	-1σ
M_*	Mass ($M_\odot$)	0.415	0.021	0.020
R_*	Radius ($R_\odot$)	0.421	0.017	0.015
L_*	Luminosity ($L_\odot$)	0.0229	0.0026	0.0023
ρ_*	Density (cgs)	7.86	0.91	0.88
$\log g$	Surface gravity (cgs)	4.809	0.034	0.037
T_{eff}	Effective Temperature (K)	3459	65	65
[Fe/H]	Metallicity (dex)	−0.07	0.11	0.11

semi-amplitude to be 37 cm s^{-1}. This small predicted signal will make a mass determination difficult, but robust upper mass limits are within reach of current instruments. A mass determination for TOI-700 e is further complicated by the fact that the orbital period (27.81 days) is very close to half that of the stellar rotation period (54 ± 0.8 days; Gilbert et al. 2020). Following the methods of Barnes et al. (2008) and using the estimated mass of 0.845 $M_\oplus$, we calculated the timescale for tidal locking of TOI-700 e to be on the order of a few million years. Given the age of the system, it is likely that the planet is in a locked-in synchronous or pseudo-synchronous rotation.

5.2. On the Habitability of TOI-700 e

The TOI-700 system is now known to contain two planets that orbit within the HZ of the host star, depicted in Figure 4. Specifically, we adopt the HZ boundaries provided by Kasting et al. (1993) and Kopparapu et al. (2013, 2014), calculated using the stellar parameters from Table 1. The HZ is broadly divided into the Conservative HZ (CHZ) and the Optimistic HZ (OHZ), described in detail by Kane et al. (2016). The CHZ

Table 2
Median Values and 68% Confidence Intervals for the Global Models of the TOI-700 Planetary Parameters

Parameter	Description (Units)	Median	$+1\sigma$	-1σ
TOI-700 b				
P	Period (days)	9.977219	0.000041	0.000038
R_P	Radius ($R_\oplus$)	0.914	0.053	0.049
T_0	Optimal conjunction time (BJD$_{TDB}$)	2458880.0993	0.0015	0.0016
a	Semimajor axis (AU)	0.0677	0.0011	0.0011
i	Inclination (Degrees)	89.60	0.27	0.29
e	Eccentricity	0.075	0.093	0.054
ω_*	Argument of periastron (Degrees)	-150	120	130
S	Insolation flux ($S_\oplus$)	4.98	0.50	0.58
R_P/R_*	Radius of planet in stellar radii	0.01993	0.00082	0.00083
T_{14}	Total transit duration (days)	0.0905	0.0036	0.0033
b	Transit impact parameter	0.24	0.19	0.16
TOI-700 c				
P	Period (days)	16.051137	0.000020	000020
R_P	Radius ($R_\oplus$)	2.60	0.14	0.13
T_0	Optimal conjunction time (BJD$_{TDB}$)	2458821.62181	0.00041	0.00042
a	Semimajor axis (AU)	0.0929	0.0015	0.0015
i	Inclination (degrees)	88.903	0.071	0.087
e	Eccentricity	0.068	0.070	0.049
ω_*	Argument of periastron (Degrees)	30	120	120
S	Insolation flux ($S_\oplus$)	2.64	0.26	0.31
R_P/R_*	Radius of planet in stellar radii	0.0565	0.0017	0.0016
T_{14}	Total transit duration (days)	0.0593	0.0017	0.0017
b	Transit impact parameter	0.899	0.014	0.017
TOI-700 e				
P	Period (days)	27.80978	0.00046	0.00040
R_P	Radius ($R_\oplus$)	0.953	0.089	0.075
T_0	Optimal conjunction time (BJD$_{TDB}$)	2458964.8112	0.0058	0.0045
a	Semimajor axis (AU)	0.1340	0.0022	0.0022
i	Inclination (Degrees)	89.60	0.21	0.16
e	Eccentricity	0.059	0.057	0.042
ω_*	Argument of periastron (Degrees)	70	100	120
S	Insolation flux ($S_\oplus$)	1.27	0.13	0.15
R_P/R_*	Radius of planet in stellar radii	0.0208	0.0017	0.0014
T_{14}	Total transit duration (days)	0.1157	0.0087	0.016
b	Transit impact parameter	0.47	0.19	0.25
TOI-700 d				
P	Period (days)	37.42396	0.00039	0.00035
R_P	Radius ($R_\oplus$)	1.073	0.059	0.054
T_0	Optimal conjunction time (BJD$_{TDB}$)	2458816.9952	0.0011	0.0013
a	Semimajor axis (AU)	0.1633	0.0027	0.0027
i	Inclination (degrees)	89.80	0.12	0.10
e	Eccentricity	0.042	0.045	0.030
ω_*	Argument of periastron (degrees)	10	120	140
S	Insolation flux ($S_\oplus$)	0.85	0.09	0.10
R_P/R_*	Radius of planet in stellar radii	0.02339	0.00077	0.00080
T_{14}	Total transit duration (days)	0.1381	0.0028	0.0023
b	Transit impact parameter	0.29	0.14	0.18

boundaries are defined by the runaway and maximum greenhouse limits, and the OHZ boundaries are based upon empirically derived estimates of when Venus and Mars may have had surface liquid water. As shown in Figure 4, planet d resides within the CHZ ($S_d = 0.85^{+0.09}_{-0.10}\ S_\oplus$; $0.246\ S_\oplus < S_{CHZ} < 0.931\ S_\oplus$) and the orbit of planet e is within the OHZ ($S_e = 1.27^{+0.13}_{-0.15}\ S_\oplus$; $0.221\ S_\oplus < S_{OHZ} < 1.493\ S_\oplus$). Systems such as TOI-700, with a potential diversity of terrestrial planetary climates, provide important context regarding climate evolution and comparative planetology (Kane et al. 2021). The insolation flux of TOI-700 e is $\sim 1.27 S_\oplus$, and thus it lies between those of Earth and Venus ($\sim 1.91 S_\oplus$). Therefore, the terrestrial planets present in the inner OHZ (planet e) and the

CHZ (planet d) serve as potential analogs to the Venus/Earth evolutions that occurred within our Solar System. The nature of the Venusian evolution remains a topic of some debate, with scenarios ranging from Venus never condensing surface liquid water (Hamano et al. 2013; Turbet et al. 2021) to Venus retaining temperate conditions until as recently as a billion years ago (Way et al. 2016; Way & Del Genio 2020). The TOI-700 system thus presents an opportunity to examine Venus within the exoplanet context (Kane et al. 2014; Barstow et al. 2016; Kane et al. 2019; Lustig-Yaeger et al. 2019; Ostberg & Kane 2019).

Within the context of planetary habitability, it is also worth noting that the planetary parameters in Table 2 show that the
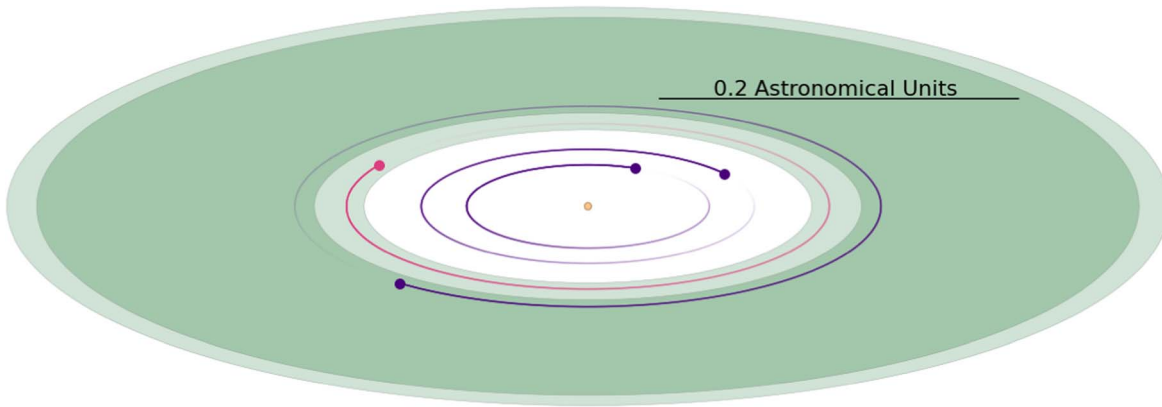
Figure 4. TOI-700 e (pink) resides in the Optimistic Habitable Zone (light green) around its host star in between the orbits of TOI-700 c and d. The Conservative Habitable Zone is shown in dark green, and planets b, c, and d (from inner to outer) are shown in indigo.

estimated orbital eccentricities are relatively low, as expected for compact multi-transiting systems (Eylen et al. 2019). Eccentricities play an important role in the evolution and stability of terrestrial planet climates (Williams & Pollard 2002; Dressing et al. 2010; Kane & Gelino 2012; Kane & Torres 2017; Way & Georgakarakos 2017). The near-circular nature of the orbits increases the likelihood of stable climates and the long-term sustainability of temperate surface conditions.

5.3. Stellar Activity and Candidate Flares

Another challenge to exoplanet habitability is the radiation environment. Low-mass stars like TOI-700 are typically highly active for long portions of their lifetimes, producing frequent flares that can alter exoplanet atmospheres. TOI-700 was first observed at 2 minutes cadence for 11 sectors during TESS Year 1 of observations. In all of these observations, there was no evidence of white-light flares in the light curves (Gilbert et al. 2020). Howard (2022) searched for flares in the 2 minutes cadence data of this target and also detected no flares.

In TESS Year 3 of observations, TOI-700 was observed for 10 full sectors of observations at 20 s cadence. This increased cadence allowed us to investigate short-lived phenomena that may not have been resolved in 2 minutes cadence data. Upon investigating the 20 s cadence data, we identified four short-duration flare candidates that were not distinguishable in the 2 minutes cadence data obtained at the same time. However, inspection of the raw 20 second data revealed that none of the candidates were flares and most were instead caused by cosmic rays hitting the detector in multiple consecutive exposures.[29]

Additional observations will help us to further characterize the magnetic activity of TOI-700. Accurate characterization of the host star is necessary for our assessment of the habitability of the planets in this system. TESS will reobserve TOI-700 beginning in 2023 January, providing us with nine more sectors of observations that may be used to study any potential activity. Additional multiwavelength and/or spectroscopic observations would also be valuable for characterizing the magnetic activity of this star. There was no evidence of flares in 15 orbits of HST observations (PI: Arney; Program: 16207) or 91 spectra taken

with ESPRESSO (PI: Gilbert; Program: 108.22C2.001). These observations will be discussed in greater detail in future papers.

5.4. Dynamical Analysis of the TOI-700 System

TOI-700 e's orbit places it conspicuously close to the interior 4:3 mean motion resonance (MMR) with TOI-700 d ($P_d/P_e =$ 1.3458). While modern theories of planet formation via pebble accretion and inward migration strongly suggest that compact systems of short-period planets form in chains of mutually resonant orbits (e.g., Izidoro et al. 2017), proximity to a resonance does not imply resonant behavior exists in a system. For instance, Jupiter and Saturn's orbital period ratio (2.49) is rather close to that of a 5:2 MMR; however, the planets are not currently in this resonance, nor is it is likely that they ever were in the past (e.g., Clement et al. 2020). Confirmation of resonant evolution in exoplanet systems requires a more precise determination of the planets' angular orbital elements and their associated frequencies via precise radial velocity campaigns and transit timing variation (TTVs; Luger et al. 2017; Leleu et al. 2021). In the absence of these data, we are forced to adopt a brute force type of methodology that interrogates the stability of the 4:3 MMR within the TOI-700 system given the current measured uncertainties on the planets' orbits. We performed a suite of 7500 N-body simulations (with a duration of 10 Myr) of the four-planet system using the `Mercury6` hybrid integrator (Chambers 1999), a 0.5 day time step, and additional forces to account for the effects of general relativity. In each individual run, we assigned the nominal orbital parameters to planets b and c, randomly varied the semimajor axes of d and e within their cataloged uncertainties, and randomly assigned an eccentricity to the outer two planets between 0.0 and 0.05 by sampling from a uniform distribution of values. While eccentricity is still not well-constrained in this system, dynamical stability considerations (Gilbert et al. 2020) strongly suggest that the eccentricities of all four planets are low. In each iteration, we initialized the longitudes of perihelia and orbital anomalies of planets e and d in a configuration that placed them well within the libration island for the 4:3 MMR. To determine whether each system evolved in MMR for the duration of the simulation, we checked for libration of the relevant resonant angles using the analysis pipeline described in Clement & Sheppard (2021). In total, 521 of our 7500 simulations (6.9%) displayed the appropriate resonant libration. However, when we restrict our sample to the 141 systems that were initialized with both planets e and d having eccentricities

---

[29] We note that, for 20 s cadence data, cosmic ray mitigation is not performed on board the spacecraft, and instead is performed in post-processing, so cosmic rays are often evident in the `raw_cnts` images from the TESS target pixel files.

less than 0.01 (which is likely the case in this system), 54 simulations produced a resonance (38%). We will be able to further assess this estimate with better constraints on the orbital parameters of the planets from ongoing radial velocity measurements and transit timing observations. While these simulations do not confirm the presence of an MMR in TOI-700, they are indeed a potential indication of the existence of one, given the aforementioned formation models and the growing sample of similar systems discovered in resonant chains.

The period ratio of 1.34 is not one that is produced in planet formation models without convergent migration and resonance capture (gas-free planetesimal accretion models tend to produce period ratios of ∼1.6–2.5; Chambers & Wetherill 1998), so it is likely that planets e and d formed in resonance as the result of orbital migration. While the system may have formed in resonance and subsequently destabilized, given the compact nature of this system and the current period ratios of the planets, it is unlikely to have experienced a scattering event under instability (Izidoro et al. 2017, 2021). Given these results, we conclude that it is quite probable that an MMR exists between planets e and d. We plan to leverage ongoing and planned observations of the system in a forthcoming manuscript, to test this assertion.

We originally explored the possibility of TTVs in the system in Gilbert et al. (2020) using a photodynamical model implemented using `TRANSITFIT5` (Rowe et al. 2015; Rowe 2016) using the first year of TESS observations. Building on this analysis, we explored the possibility of TTVs within this system by analyzing the additional year of observations with the new planet, TOI-700 e, using the `TTVFast` Python package. We modeled a variety of conditions for all four planets, sampling over a range of orbital eccentricities and planet masses. In 1,000 realizations of the system, planets b and c only show small TTVs at most (on the order of a few minutes). Planets e and d show potentially larger variations (TTVs of up to a few hours), as a result of near-resonant TTV behavior if eccentricity is as high as 0.05, but we do not see evidence of such large TTVs in the TESS photometry. We measured the TTVs for both planets; they are consistent with 0 within errors and have an rms of 24 minutes for planet d and 1 hr for planet e. This means that the eccentricities of the TOI-700 planets are likely very low, as one would expect for a compact, multi-planet system. Future transit observation with TESS and ongoing radial velocity measurements with ESPRESSO will help us to further constrain the orbital parameters of the planets in this system. These radial velocity measurements will also allow us to determine the masses of the TOI-700 planets and place further constraints on expected TTV amplitudes.

5.5. Comparison to Other Multi-planet Systems

The TESS mission has so far discovered over 100 planets in multi-planet systems, the majority of which orbit M-dwarf stars. The L 98-59 (TOI-175) system was one of the earliest multi-planet systems discovered using TESS (Kostov et al. 2019a), and it contains three terrestrial-sized, transiting planets (and at least one nontransiting planet; Demangeon et al. 2021). L 98-59 is a bright ($V = 11.7$ mag), nearby (10.6 pc) M3 dwarf that exhibits moderate amounts of activity in TESS optical light curves. L 231-32 (TOI-270) also hosts multiple transiting planets that were discovered in TESS data (Günther

et al. 2019). L 231-32 is also an M3 dwarf and hosts three super-Earth to sub-Neptune-sized planets orbiting close to the star. L 98-59 was observed with HARPS (Cloutier et al. 2019), and both the L 98-59 and L 231-32 systems were subsequently followed up with ESPRESSO in order to obtain precise measurements of planet mass (Demangeon et al. 2021; Van Eylen et al. 2021, respectively). TESS also revealed the presence of three planets around M0 dwarf TOI-1749 (Fukui et al. 2021), ranging from super-Earth to sub-Neptune in size. These systems with multiple transiting planets are all likely coplanar, given their geometries. Indeed, the inclinations of the TOI-700 planets are consistent with each other and are comparable to the inclinations of solar system planets.

TOI-700 adds to the growing number of multi-planet systems discovered using TESS. Now with a second small, HZ planet known to orbit this star, this system is worthy of further investigation. Multi-planetary systems that harbor small planets in or near the HZ and orbit stars bright enough for follow-up atmospheric characterization are quite rare. There are only a few dozen multi-planet systems that host temperate worlds. Even fewer of these worlds are small enough to be rocky or orbit stars bright enough for detailed follow-up observations.

Famously, TRAPPIST-1 hosts seven known transiting planets (Gillon et al. 2017), several of which reside within the star's HZ. Comparing between the TOI-700 and TRAPPIST-1 systems with their multiple small, HZ planets provides us with valuable insight into what processes affect planetary habitability besides simply insolation flux. We are able to compare between host stars on either side of the convective boundary, as well as host stars that are quiet (TOI-700) versus active (TRAPPIST-1). In these systems with multiple HZ planets, we know that the planets' host stars are the same, so their evolutionary histories are well-controlled and any differences in habitability can be attributed to phenomena other than the star's radiation environment or evolution.

5.6. Prospects for Future Investigations

We conducted a transit search on our reduced light curves (described in Section 2.1) and did not identify any additional signals (beyond the ones already detected) that may be indicative of other planets in the system. However, TESS will reobserve TOI-700 for nine sectors in its upcoming Cycle 5 observations. Additional photometry may reveal additional low-signal planets in this system, as could ongoing ESPRESSO precision radial velocity measurements (Programs 108.22C2.001 and 110.242P.001, PI: Gilbert), which will be discussed in a forthcoming paper (E. A. Gilbert et al. 2023, in preparation).

In the absence of extracted RV masses at this point in time, we used Chen & Kipping (2017) mass estimates to calculate the transmission spectroscopy metric (TSM; Kempton et al. 2018) for each of the TOI-700 planets to be 4 (planet b), 76 (planet c), 4 (planet e), and 3 (planet d). For reference, TOI-700 e receives an insolation flux 1.25 times that of Earth's irradiance, which is between those of TRAPPIST-1 c (2.27 $S_\oplus$) and TRAPPIST-1 d (1.143 $S_\oplus$) (Gillon et al. 2017). TRAPPIST-1 c and d have significantly higher TSM values (26 and 24, respectively) because of the comparatively smaller size of their host star. However, it is worth revisiting these metrics once we have precisely measured masses for the TOI-700 planets, to fully assess their observability.

6. Conclusions

We present the discovery of a new, small planet orbiting within the HZ of TOI-700 called TOI-700 e. TOI-700 e is a 0.95 $R_\oplus$ planet that orbits its host star every 27.8 days. Due to its small size, this planet was not detected in Year 1 of TESS observations alone, but data from the TESS extended mission revealed its existence. TOI-700 e orbits interior to TOI-700 d (Gilbert et al. 2020; Rodriguez et al. 2020) and receives 1.27× Earth's insolation flux (as compared to 0.86 for TOI-700 d), putting it within the star's Optimistic HZ. TOI-700 e has a low-eccentricity orbit, likely rotates in a synchronized state with its 27.8 day orbit, and may be in a mean motion resonance with its fellow Earth-sized, HZ planet, TOI-700 d.

TOI-700 is a notable system because it hosts multiple small planets, two of which are now known to orbit within the star's habitable zone. Most importantly, TOI-700 is relatively quiet and bright enough that we can now take the next steps to further characterize this system and learn more about its HZ planets. This lack of activity is also greatly beneficial in terms of planetary habitability. We see no signs of flares in the TESS optical photometry, and TOI-700 is quiet when observed by HST in the UV, which is valuable in terms of planets' abilities to retain their atmospheres over time. TOI-700 will present an important contrast to other systems, such as TRAPPIST-1, that host small, HZ planets but have higher levels of stellar activity. A comparison between these planets may elucidate how the stellar environment affects planets' ability to maintain their atmospheres and what their compositions are like. The more systems we can study with multiple HZ planets, the better our understanding of these worlds will be.

Facilities: CAO, TESS.

Software: DAVE (Kostov et al. 2019b), exofast (Eastman et al. 2013, 2019) Forecaster (Chen & Kipping 2017), Jupyter (Pérez & Granger 2007), Lightkurve (Lightkurve Collaboration et al. 2018), Matplotlib (Hunter 2007), Mercury6 (Chambers 1999), NumPy (van der Walt et al. 2011), Pandas (McKinney et al. 2010), TTVFast (Deck et al. 2014), vespa (Morton 2012, 2015), xoflares (Barclay & Gilbert 2020).

ORCID iDs

Emily A. Gilbert ⓘ https://orcid.org/0000-0002-0388-8004
Andrew Vanderburg ⓘ https://orcid.org/0000-0001-7246-5438
Joseph E. Rodriguez ⓘ https://orcid.org/0000-0001-8812-0565
Benjamin J. Hord ⓘ https://orcid.org/0000-0003-3904-6754
Matthew S. Clement ⓘ https://orcid.org/0000-0001-8933-6878
Thomas Barclay ⓘ https://orcid.org/0000-0001-7139-2724
Elisa V. Quintana ⓘ https://orcid.org/0000-0003-1309-2904
Joshua E. Schlieder ⓘ https://orcid.org/0000-0001-5347-7062
Stephen R. Kane ⓘ https://orcid.org/0000-0002-7084-0529
Jon M. Jenkins ⓘ https://orcid.org/0000-0002-4715-9460
Joseph D. Twicken ⓘ https://orcid.org/0000-0002-6778-7552
Michelle Kunimoto ⓘ https://orcid.org/0000-0001-9269-8060
Roland Vanderspek ⓘ https://orcid.org/0000-0001-6763-6562
Giada N. Arney ⓘ https://orcid.org/0000-0001-6285-267X
David Charbonneau ⓘ https://orcid.org/0000-0002-9003-484X
Maximilian N. Günther ⓘ https://orcid.org/0000-0002-3164-9086
Chelsea X. Huang ⓘ https://orcid.org/0000-0003-0918-7484
Giovanni Isopi ⓘ https://orcid.org/0000-0002-8458-0588
Veselin B. Kostov ⓘ https://orcid.org/0000-0001-9786-1031
Martti H. Kristiansen ⓘ https://orcid.org/0000-0002-2607-138X
David W. Latham ⓘ https://orcid.org/0000-0001-9911-7388
Franco Mallia ⓘ https://orcid.org/0000-0001-5724-1807

Eric E. Mamajek ● https://orcid.org/0000-0003-2008-1488
Ismael Mireles ● https://orcid.org/0000-0002-4510-2268
Samuel N. Quinn ● https://orcid.org/0000-0002-8964-8377
George R. Ricker ● https://orcid.org/0000-0003-2058-6662
Jack Schulte ● https://orcid.org/0000-0002-7382-0160
S. Seager ● https://orcid.org/0000-0002-6892-6948
Gabrielle Suissa ● https://orcid.org/0000-0003-4471-1042
Joshua N. Winn ● https://orcid.org/0000-0002-4265-047X
Allison Youngblood ● https://orcid.org/0000-0002-1176-3391
Aldo Zapparata ● https://orcid.org/0000-0002-9428-1573

References

Auvergne, M., Bodin, P., Boisnard, L., et al. 2009, A&A, 506, 411
Barclay, T., & Gilbert, E. 2020, mrtommyb/xoflares v0.2.1, Zenodo, doi:10.5281/zenodo.4156285
Barnes, R., Raymond, S. N., Jackson, B., & Greenberg, R. 2008, AsBio, 8, 557
Barstow, J. K., Aigrain, S., Irwin, P. G. J., Kendrew, S., & Fletcher, L. N. 2016, MNRAS, 458, 2657
Benz, W., Broeg, C., Fortier, A., et al. 2021, ExA, 51, 109
Borucki, W. J., Koch, D., Basri, G., et al. 2010, Sci, 327, 977
Bouchy, F., Udry, S., Mayor, M., et al. 2005, A&A, 444, L15
Bryson, S., Kunimoto, M., Kopparapu, R. K., et al. 2021, AJ, 161, 36
Bryson, S. T., Jenkins, J. M., Gilliland, R. L., et al. 2013, PASP, 125, 889
Chambers, J. E. 1999, MNRAS, 304, 793
Chambers, J. E., & Wetherill, G. W. 1998, Icar, 136, 304
Chen, J., & Kipping, D. 2017, ApJ, 834, 17
Clement, M. S., Morbidelli, A., Raymond, S. N., & Kaib, N. A. 2020, MNRAS, 492, L56
Clement, M. S., & Sheppard, S. S. 2021, AJ, 162, 27
Cloutier, R., Astudillo-Defru, N., Bonfils, X., et al. 2019, A&A, 629, A111
Deck, K. M., Agol, E., Holman, M. J., & Nesvorný, D. 2014, ApJ, 787, 132
Demangeon, O. D. S., Zapatero Osorio, M. R., Alibert, Y., et al. 2021, A&A, 653, A41
Dressing, C. D., & Charbonneau, D. 2013, ApJ, 767, 95
Dressing, C. D., & Charbonneau, D. 2015, ApJ, 807, 45
Dressing, C. D., Spiegel, D. S., Scharf, C. A., Menou, K., & Raymond, S. N. 2010, ApJ, 721, 1295
Eastman, J., Gaudi, B. S., & Agol, E. 2013, PASP, 125, 83
Eastman, J. D., Rodriguez, J. E., Agol, E., et al. 2019, arXiv:1907.09480
Eylen, V. V., Albrecht, S., Huang, X., et al. 2019, AJ, 157, 61
Fazio, G. G., Hora, J. L., Allen, L. E., et al. 2004, ApJS, 154, 10
Fukui, A., Korth, J., Livingston, J. H., et al. 2021, AJ, 162, 167
Gilbert, E. A., Barclay, T., Schlieder, J. E., et al. 2020, AJ, 160, 116
Gillon, M., Triaud, A. H. M. J., Demory, B.-O., et al. 2017, Natur, 542, 456
Girardi, L., Groenewegen, M., Hatziminaoglou, E., & Da Costa, L. 2005, A&A, 436, 895
Guerrero, N. M., Seager, S., Huang, C. X., et al. 2021, ApJS, 254, 39
Günther, M. N., Pozuelos, F. J., Dittmann, J. A., et al. 2019, NatAs, 3, 1099
Hamano, K., Abe, Y., & Genda, H. 2013, Natur, 497, 607
Howard, W. S. 2022, MNRAS, 512, L60
Hunter, J. D. 2007, CSE, 9, 90
Izidoro, A., Bitsch, B., Raymond, S. N., et al. 2021, A&A, 650, A152
Izidoro, A., Ogihara, M., Raymond, S. N., et al. 2017, MNRAS, 470, 1750
Jenkins, J. M., Caldwell, D. A., & Borucki, W. J. 2002, ApJ, 564, 495
Jenkins, J. M., Tenenbaum, P., Seader, S., et al. 2020, Kepler Data Processing Handbook: Transiting Planet Search, Kepler Science Document KSCI-19081-003, 9
Jenkins, J. M., Radziwill, N. M., Bridger, A., et al. 2010, Proc. SPIE, 7740, 77400D

Jenkins, J. M., Twicken, J. D., McCauliff, S., et al. 2016, Proc. SPIE, 9913, 99133E
Kane, S. R., & Gelino, D. M. 2012, AsBio, 12, 940
Kane, S. R., Arney, G., Crisp, D., et al. 2019, JGRE, 124, 2015
Kane, S. R., Hill, M. L., Kasting, J. F., et al. 2016, ApJ, 830, 1
Kane, S. R., Kopparapu, R. K., & Domagal-Goldman, S. D. 2014, ApJL, 794, L5
Kane, S. R., Li, Z., Wolf, E. T., Ostberg, C., & Hill, M. L. 2021, AJ, 161, 31
Kane, S. R., & Torres, S. M. 2017, AJ, 154, 204
Kasting, J. F., Whitmire, D. P., & Reynolds, R. T. 1993, Icar, 101, 108
Kempton, E.-M.-R., Bean, J. L., Louie, D. R., et al. 2018, PASP, 130, 114401
Kirkpatrick, J. D., Henry, T. J., & McCarthy, D. W., Jr. 1991, ApJS, 77, 417
Kopparapu, R. K., Ramirez, R. M., SchottelKotte, J., et al. 2014, ApJL, 787, L29
Kopparapu, R. K., Ramirez, R., Kasting, J. F., et al. 2013, ApJ, 765, 131
Kostov, V. B., Mullally, S. E., Quintana, E. V., et al. 2019b, arXiv:1901.07459
Kostov, V. B., Schlieder, J. E., Barclay, T., et al. 2019a, AJ, 158, 32
Leleu, A., Alibert, Y., Hara, N. C., et al. 2021, A&A, 649, A26
Li, J., Tenenbaum, P., Twicken, J. D., et al. 2019, PASP, 131, 024506
Lightkurve Collaboration, Cardoso, J. V. d., Hedges, C., et al. 2018, Lightkurve: Kepler and TESS time series analysis in Python, Astrophysics Source Code Library, ascl:1812.013
Lissauer, J. J., Marcy, G. W., Bryson, S. T., et al. 2014, ApJ, 784, 44
Lissauer, J. J., Marcy, G. W., Rowe, J. F., et al. 2012, ApJ, 750, 112
Luger, R., Sestovic, M., Kruse, E., et al. 2017, NatAs, 1, 0129
Lustig-Yaeger, J., Meadows, V. S., & Lincowski, A. P. 2019, ApJL, 887, L11
Mann, A. W., Feiden, G. A., Gaidos, E., Boyajian, T., & Braun, K. v. 2015, ApJ, 804, 64
Mayor, M., Marmier, M., Lovis, C., et al. 2011, arXiv:1109.2497
Mayor, M., Pepe, F., Queloz, D., et al. 2003, Msngr, 114, 20
Mayor, M., & Queloz, D. 1995, Natur, 378, 355
McKinney, W. 2010, in Proc. of the 9th Python in Science Conf. 445, ed. S. van der Walt & J. Millman (Austin, TX: SciPy), 51
Morton, T. D. 2012, ApJ, 761, 6
Morton, T. D. 2015, VESPA: False positive probabilities calculator, Astrophysics Source Code Library, ascl:1503.011
Ostberg, C., & Kane, S. R. 2019, AJ, 158, 195
Perez, F., & Granger, B. E. 2007, CSE, 9, 21
Petigura, E. A., Howard, A. W., & Marcy, G. W. 2013, PNAS, 110, 19273
Quintana, E. V., Barclay, T., Raymond, S. N., et al. 2014, Sci, 344, 277
Raghavan, D., McAlister, H. A., Henry, T. J., et al. 2010, ApJS, 190, 1
Ricker, G. R., Winn, J. N., Vanderspek, R., et al. 2015, JATIS, 1, 014003
Rodriguez, J. E., Vanderburg, A., Zieba, S., et al. 2020, AJ, 160, 117
Rowe, J. 2016, Kepler: Kepler Transit Model Codebase Release. v1.0, Zenodo, doi:10.5281/zenodo.60297
Rowe, J. F., Coughlin, J. L., Antoci, V., et al. 2015, ApJS, 217, 16
Smith, J. C., Stumpe, M. C., Van Cleve, J. E., et al. 2012, PASP, 124, 1000
Stumpe, M. C., Smith, J. C., Catanzarite, J. H., et al. 2014, PASP, 126, 100
Stumpe, M. C., Smith, J. C., Van Cleve, J. E., et al. 2012, PASP, 124, 985
Turbet, M., Bolmont, E., Chaverot, G., et al. 2021, Natur, 598, 276
Twicken, J. D., Catanzarite, J. H., Clarke, B. D., et al. 2018, PASP, 130, 064502
van der Walt, S., Colbert, S. C., & Varoquaux, G. 2011, CSE, 13, 22
Van Eylen, V., Astudillo-Defru, N., Bonfils, X., et al. 2021, MNRAS, 507, 2154
Vanderburg, A., Huang, C. X., Rodriguez, J. E., et al. 2019, ApJL, 881, L19
Walker, G., Matthews, J., Kuschnig, R., et al. 2003, PASP, 115, 1023
Way, M. J., & Del Genio, A. D. 2020, JGRE, 125, e06276
Way, M. J., Del Genio, A. D., Kiang, N. Y., et al. 2016, GeoRL, 43, 8376
Way, M. J., & Georgakarakos, N. 2017, ApJL, 835, L1
Williams, D. M., & Pollard, D. 2002, IJAsB, 1, 61
Wolszczan, A., & Frail, D. A. 1992, Natur, 355, 145